

WHAT LURKS IN THE MARTIAN ROCKS AND SOIL? INVESTIGATIONS OF SULFATES, PHOSPHATES, AND PERCHLORATES

Spectral properties of Ca-sulfates: Gypsum, bassanite, and anhydrite†

JANICE L. BISHOP^{1,*}, MELISSA D. LANE², M. DARBY DYAR³, SARA J. KING¹, ADRIAN J. BROWN¹ AND GREGG A. SWAYZE⁴

¹SETI Institute, Carl Sagan Center, Mountain View, California 94043, U.S.A.

²Planetary Science Institute, 1700 E. Fort Lowell Road, Suite 106, Tucson, Arizona 85719, U.S.A.

³Department of Astronomy, Mount Holyoke College, South Hadley, Massachusetts 01075, U.S.A.

⁴U.S. Geological Survey, Denver, Colorado 80225, U.S.A.

ABSTRACT

This study of the spectral properties of Ca-sulfates was initiated to support remote detection of these minerals on Mars. Gypsum, bassanite, and anhydrite are the currently known forms of Ca-sulfates. They are typically found in sedimentary evaporites on Earth, but can also form via reaction of acidic fluids associated with volcanic activity. Reflectance, emission, transmittance, and Raman spectra are discussed here for various sample forms. Gypsum and bassanite spectra exhibit characteristic and distinct triplet bands near 1.4–1.5 μm , a strong band near 1.93–1.94 μm , and multiple features near 2.1–2.3 μm attributed to H₂O. Anhydrite, bassanite, and gypsum all have SO₄ combination and overtone features from 4.2–5 μm that are present in reflectance spectra. The mid-IR region spectra exhibit strong SO₄ ν_3 and ν_4 vibrational bands near 1150–1200 and 600–680 cm^{-1} (~8.5 and 16 μm), respectively. Additional weaker features are observed near 1005–1015 cm^{-1} (~10 μm) for ν_1 and near 470–510 cm^{-1} (~20 μm) for ν_2 . The mid-IR H₂O bending vibration occurs near 1623–1630 cm^{-1} (~6.2 μm). The visible/near-infrared region spectra are brighter for the finer-grained samples. In reflectance and emission spectra of the mid-IR region the ν_4 bands begin to invert for the finer-grained samples, and the ν_1 vibration occurs as a band instead of a peak and has the strongest intensity for the finer-grained samples. The ν_2 vibration is a sharp band for anhydrite and a broad peak for gypsum. The band center of the ν_1 vibration follows a trend of decreasing frequency (increasing wavelength) with increasing hydration of the sample in the transmittance, Raman, and reflectance spectra. Anhydrite forms at elevated temperatures compared to gypsum, and at lower temperature, salt concentration, and pH than bassanite. The relative humidity controls whether bassanite or gypsum is stable. Thus, distinguishing among gypsum, bassanite, and anhydrite via remote sensing can provide constraints on the geochemical environment.

Keywords: Gypsum, sulfate, reflectance spectra, emission spectra, infrared

INTRODUCTION

Common forms of Ca-sulfate are anhydrite CaSO₄, bassanite CaSO₄·0.5H₂O, and gypsum CaSO₄·2H₂O (e.g., Dyar et al. 2008). Anhydrite typically forms at higher temperatures and gypsum at lower temperatures (Hardie 1967; Deer et al. 1992) and transformations between these two forms of Ca-sulfates do not occur readily under dry conditions at low temperatures. Gypsum, bassanite, and anhydrite are all common sedimentary minerals found in marine evaporite sequences on Earth (Prothero and Schwab 2004). They can also occur as hydrothermal veins (Deer et al. 1992). Ca-sulfates have important industrial applications and are components of drywall, plaster, and cement (e.g., Singh and Garg 1995; Dyar et al. 2008).

Gypsum is one of the first minerals precipitated from seawater of normal salinity because Ca²⁺ and SO₄²⁻ are less soluble than

other ions. Thick, extensive gypsum deposits are less common than smaller outcrops, but are observed in shallow basin environments (Hardie and Eugster 1971). Gypsum generally forms at temperatures below 60 °C (Conley and Bundy 1958), while anhydrite forms at elevated temperatures and increased Ca²⁺ and SO₄²⁻ brine concentration (Billo 1987). Gypsum can also form from sulfuric acid solution or vapors through fumarole activity, and it is also found in ash and ejecta blocks (Belousov 1995; Holland 2002). Bassanite is characteristic of dry marine evaporitic environments (Gunatilaka et al. 1985) and dry lake beds (Allen and Kramer 1953).

Gypsum and bassanite have been detected in several regions on Mars in data from the Compact Reconnaissance Imaging Spectrometer for Mars (CRISM) data (e.g., Murchie et al. 2009) and the Observatoire pour la Minéralogie, l'Eau, les Glaces et l'Activité (OMEGA) data (e.g., Bibring et al. 2005) using the characteristic near-infrared (NIR) spectral features near 1.5, 1.9, and 2.2 μm . Because pure anhydrite spectra do not contain features in this range, it is more difficult to detect anhydrite in CRISM and OMEGA images. The SO₄ overtones and combinations observed

* E-mail: jbishop@seti.org

† Special collection papers can be found on GSW at <http://ammin.geoscienceworld.org/site/misc/specialissuelist.xhtml>.

from 4.2–5 μm are included in the spectral range covered by OMEGA; however, features in this range for Ca-sulfates have not yet been observed on Mars. This spectral region poses additional challenges because both reflectance and thermal emission contribute to the spectra here (Blaney and McCord 1995; Sutter et al. 2007; Witzke et al. 2007). The Thermal Emission Spectrometer (TES) data cover the spectral range \sim 5.8–50 μm or 200–1724 cm^{-1} where the fundamental SO_4 vibrations are observed. Sulfates are often present at minor abundances in the TES model results, but at levels below what is needed to confidently identify them in the surface material (Christensen et al. 2001), possibly because the sulfate features occur in the same spectral range as the atmospheric and surface dust that are confounding sulfate identification. The dust may also contain some sulfate. If the sulfates are fine grained that would result in shallow diagnostic features as well, which would be difficult to discern.

Gypsum is the most common form of Ca-sulfate found on Mars. It has been identified at Olympia Undae (Langevin et al. 2005; Fishbaugh et al. 2007; Szumila et al. 2013), Meridiani Planum (Grotzinger et al. 2005; Squyres 2012), and Noctis Labyrinthus (Weitz et al. 2013). Bassanite has been found at Mawrth Vallis (Wray et al. 2010).

The spectral properties of anhydrite, bassanite and gypsum are useful for remote detection of these minerals on the Earth and Mars. Many past studies have presented data of these minerals individually for a limited wavelength region (Miller and Wilkins 1952; Miller et al. 1960; Moenke 1962; Hunt et al. 1971; Ross 1974; McMillan and Hofmeister 1988; Crowley 1991; Bishop et al. 2004; Lane 2007; Harrison 2012) or published the spectra as part of a library without interpretation of the spectral features (Salisbury et al. 1991; Clark et al. 2007). The objective of this study is to present a coordinated analysis of the spectral features of all three Ca-sulfate minerals with respect to their structures across the visible and infrared regions where remotely sensed spectra are used for detection of these minerals. Through coordinated analysis of the mid-infrared fundamental vibrations and the near-infrared overtones and combinations, band assignments can be made and confirmed.

BACKGROUND

Gypsum is the most common sulfate mineral and has been known since the time of the Greeks (e.g., Bromehead 1943). Gypsum occurs as clear crystals called selenite or as massive material called alabaster. Anhydrite was named after the Greek word for “without water” (Ludwig 1804) and can be vitreous, greasy, and pearly. Both gypsum and anhydrite are prevalent in evaporite deposits of marine origin in numerous sites on Earth (e.g., Billo 1987). Anhydrite is harder and more dense than gypsum (e.g., Deer et al. 1992); δ_{gypsum} is $\approx 2.3 \text{ g/cm}^3$, whereas $\delta_{\text{anhydrite}}$ is $\approx 2.9 \text{ g/cm}^3$ (Robertson et al. 1958). Gypsum is the main constituent of the dunes at the White Sands National Monument in New Mexico (e.g., Szykiewicz et al. 2010) and is present at 95–99 wt% in much of the dune sand (Fenton et al. 2014; Lafuente et al. 2014).

Particulate anhydrite will slowly react to form gypsum at low temperatures when water is added, making it a useful component of cement (e.g., Sievert et al. 2005). Gypsum and anhydrite are often located together when large marine evaporite deposits were formed under variable temperatures (Appleyard 1983; Haynes

et al. 1989). Halite is also frequently found with anhydrite and gypsum when the evaporitic brine contains Na^+ , Ca^{2+} , Cl^- , and SO_4^{2-} (e.g., Posnjak 1940; Robertson et al. 1958; Leitner et al. 2013).

Bassanite was originally found in volcanic settings as leucite tephra blocks at Vesuvius, Italy, and was named after Francesco Bassani (Zambonini 1910). Bassanite is also known as plaster of Paris and as hemihydrate (e.g., Singh and Middendorf 2007). It has been found in dry lake beds in California (Allen and Kramer 1953), in rocks along the coast of England (Worku and Parker 1992), Indiana (Bundy 1956), and the Arabian Gulf (Gunatilaka et al. 1985). Bassanite is a metastable mineral that forms when gypsum and anhydrite are in transition (Bundy 1956) and frequently occurs following dissolution and reprecipitation of gypsum (Worku and Parker 1992). Bassanite is present in marine evaporitic environments in the dry summer season in Kuwait and hydrates to gypsum in the wet winter months (Gunatilaka et al. 1985).

Mineral structures of Ca-sulfates

Gypsum, bassanite and anhydrite are all monoclinic (e.g., Dyar et al. 2008). The structures are based on large coordination polyhedra needed to accommodate the Ca^{2+} cation, so Ca is generally 8- or 9-coordinated. Most forms of Ca-sulfates are variations on the anhydrite structure, which consists of alternating chains of Ca dodecahedra sharing edges with SO_4 tetrahedra (e.g., Dyar et al. 2008). As seen in Figure 1, bassanite and gypsum represent slight variations on the anhydrite structure. In bassanite, the Ca cation is 9-coordinated, and the chains of alternating edge-sharing trigonal prisms and sulfate tetrahedra connect to form a framework. The gypsum structure is quite similar to that of anhydrite, although the repeat distance between the chains is slightly longer for gypsum and O^{2-} is replaced by H_2O at two of the unshared corners of each 8-coordinated Ca site. The compactness of these structures depends on how many H_2O groups are in each mineral, and on the number of alkali elements (Hawthorne et al. 2000). Anhydrite and bassanite have no or 0.5 H_2O per unit formula, respectively, and the chains are linked into three-dimensional frameworks. Gypsum has 2 H_2O

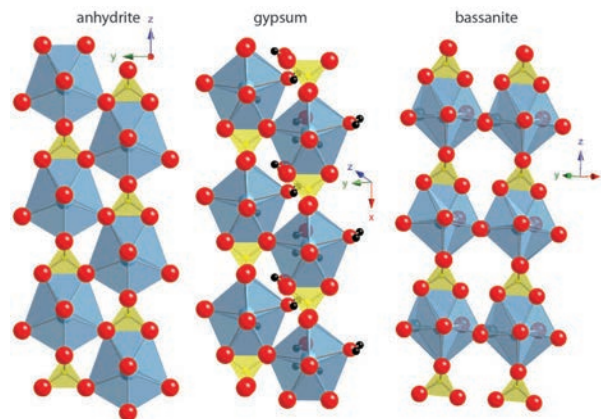


FIGURE 1. Comparison of the structures of anhydrite, bassanite, and gypsum, which are all based on the large coordination polyhedron of the Ca^{2+} cation. All three structures consist of Ca polyhedra sharing edges with SO_4 tetrahedra to form chains. The structures differ by how the chains are connected, and by how many corners of the Ca polyhedra are shared with H_2O . (Color online.)

molecules per formula unit, resulting in a sheet structure with H-bonding between water molecules in adjacent chains.

Bassanite generally exists as monoclinic α -hemihydrate but can also exist as triclinic β -hemihydrate when formed in specific synthetic environments (Singh and Middendorf 2007). The α -hemihydrate is formed from gypsum at temperatures above 45 °C in acidic environments or salt solutions or above 97 °C in water and is the most common form of bassanite. The β -hemihydrate is made by calcining gypsum under low-water vapor pressure or under vacuum at 45–200 °C (Singh and Middendorf 2007).

Spectral properties of Ca-sulfates

Early visible/near-infrared (VNIR) reflectance spectra of sulfates were presented by Hunt et al. (1971) and illustrated that the dominant VNIR bands are due to H₂O near 1.4–1.5 and 1.9–2.0 μm . More recent NIR sulfate spectra demonstrated that both OH and H₂O are responsible for most features in the 1–3 μm range (Clark et al. 1990; Crowley 1991; Bishop and Murad 1996, 2005; Cloutis et al. 2006); however, features near 4.3–5.3 μm are attributed to overtones and combinations of the ν_3 SO₄ asymmetric stretching vibration (Blaney and McCord 1995; Bishop and Murad 2005). Hunt et al. (1971) identified bands near 1.0, 1.2, 1.4–1.5, 1.75, and 1.9–2.0 μm in spectra of gypsum. Crowley (1991) showed that bassanite spectra have similar features to gypsum spectra, but that many bands are sufficiently distinct for differentiation of these minerals. Experiments by Harrison (2012) showed that the characteristic gypsum bands shift toward shorter wavelengths as the sample is converted to bassanite. However, the specific wavelengths of each of these features in gypsum and bassanite spectra have not been presented and analyzed in past studies. Anhydrite should be anhydrous and thus featureless near 1.4 and 1.9 μm , but spectra of many “anhydrite” specimens do show weak features here indicating that they are partially hydrated and possibly in transition to bassanite or gypsum (Cloutis et al. 2006).

Mid-infrared (mid-IR) transmission spectra of sulfates were summarized by Ross (1974) and include features near 980 cm^{-1} for the SO₄ ν_1 symmetric stretching vibration, near 450 cm^{-1} for the SO₄ ν_2 symmetric bending vibration, near 1100 cm^{-1} for ν_3 and near 610 cm^{-1} for the SO₄ ν_4 asymmetric bending vibration. Early studies of gypsum spectra describe strong bands at 603, 668, 1130, 1630, 2200, and 3410 cm^{-1} , plus weak bands at 1010 and 1670 cm^{-1} (Miller and Wilkins 1952; Miller et al. 1960). The frequencies of the ν_1 , ν_2 , ν_3 , and ν_4 sulfate modes are generally similar for all Ca-sulfates in transmission (Moenke 1962), Raman (Prasad et al. 2001), and emission (Lane 2007) data. Small shifts toward higher frequencies were observed for ν_1 and ν_2 from gypsum to bassanite to anhydrite in transmission spectra (Moenke 1962; Ross 1974). Triplets were observed near 1100–1150 cm^{-1} for ν_3 and near 590–675 cm^{-1} for ν_4 in all Ca-sulfate spectra (Moenke 1962; Ross 1974), and this relative shift to higher frequencies with less water in the structure was seen in emission data for the ν_3 and lattice modes (Lane 2007). Additional H₂O stretching ($\nu\text{H}_2\text{O}$) features are observed for bassanite near 3465 and 3615 cm^{-1} and for gypsum at 3250, 3408, 3500, and 3555 cm^{-1} , and H₂O bending ($\delta\text{H}_2\text{O}$) vibrations occur at 1629 cm^{-1} for bassanite and at 1629 and 1690 cm^{-1} for gypsum (Ross 1974) in the transmission data. Mid-IR emission data show the $\delta\text{H}_2\text{O}$ band at \sim 1630 cm^{-1} for bassanite and at 1621 cm^{-1} for gypsum (Lane 2007).

Raman spectra of gypsum, bassanite, and anhydrite exhibit similar trends with a single absorption due to the ν_1 vibration present at 1004–1016 cm^{-1} , ν_2 as a doublet near 414–438 and 490–498 cm^{-1} , ν_3 as a triplet near 1110–1160 cm^{-1} , and ν_4 as a triplet at \sim 602–670 cm^{-1} (Berenblut et al. 1973; Prasad et al. 2001, 2005).

Formation and stability of Ca-sulfates

Early investigations of marine evaporites suggested that gypsum was always deposited first and then partially converted to anhydrite in some cases (e.g., Murray 1964). However, Billo (1987) noted that many ancient marine evaporite deposits contain anhydrite at depth with gypsum on the surface or alternating laminae of anhydrite and other minerals, suggesting that other formation paths exist for anhydrite. It can form as a primary evaporative mineral under conditions of elevated temperatures, increased Ca²⁺ and SO₄²⁻ brine concentration and/or the presence of organic matter (Billo 1987). Experiments by Meijer (1984) on Ca-sulfate solubility at variable temperature, pH, and salt concentration of seawater showed that gypsum precipitation is favored at 1 atm where there are high salt concentrations and temperatures below 40 °C, while anhydrite generally forms at temperatures \sim 40–120 °C and pH \sim 6–7. Bassanite forms at higher temperatures (favored above 120 °C, but possible above 80 °C) than anhydrite and at a higher pH range of \sim 8–9. Generally anhydrite forms under lower salt concentrations and bassanite at higher salt concentrations. However, anhydrite becomes less soluble than bassanite and will preferentially precipitate out at a pH of 6 even for higher salt concentrations.

Many researchers have studied the transformation of gypsum and anhydrite and found that gypsum is more prevalent at lower temperatures, while anhydrite is the stable form at higher temperatures (e.g., Ostroff 1964; Innorta et al. 1980; Kushnir 1982; Zhang et al. 1996; Sievert et al. 2005). Early experiments showed that conversion occurs as gypsum changes to bassanite and then anhydrite (Conley and Bundy 1958; Ostroff 1964). Ostroff (1964) found that particulate gypsum reacted in salt solution at 90 °C to form anhydrite in a few days, whereas the reaction of gypsum in pure Ca-sulfate solution required temperatures above 97 °C. Gypsum and bassanite were converted to anhydrite in brine solution at 83 °C, where the gypsum needles were clearly observed to disappear as tiny anhydrite crystals were formed (Kushnir 1982). These experiments demonstrated that formation of bassanite was not a requirement in the phase transformation from gypsum to anhydrite, as confirmed by Prasad et al. (2005). Another study showed that bassanite will never form below \sim 88 °C (Ridge and Beretka 1969). Billo (1987) observed that gypsum can be converted to bassanite in pure water at temperatures over 100 °C and then converted to anhydrite, but that bassanite cannot be derived from anhydrite at any temperature. Anhydrite can be dissolved in solution and then reprecipitated as gypsum under low-temperature conditions. Sievert et al. (2005) studied gypsum formation from anhydrite in solution and found that this was faster at temperatures below 40 °C. However, the anhydrite must be at least partially dissolved first; gypsum cannot be formed directly by hydrating anhydrite (e.g., Prasad et al. 2005).

Innorta et al. (1980) investigated gypsum solubility in pure water and found an equilibrium temperature of 49.5 ± 2.5 °C, while Hardie (1967) found the equilibrium temperature for gyp-

sum and anhydrite solubilities to be 58 °C. Billo (1987) states that kinetic considerations are also important in understanding gypsum-anhydrite equilibria in solution and that grain size and hardness contribute to the solubility of Ca-sulfates.

Conversion of anhydrite to gypsum has been studied in detail by the cement industry. Singh and Garg (1995) describe a dissolution-nucleation growth process where Ca is separated from SO₄ in anhydrite by activator salts and then gypsum is precipitated as the Ca and sulfate react again in solution. Experiments by Sievert et al. (2005) suggest that partially dissolved anhydrite grains serve as nucleation centers for adsorbed hydrated Ca-sulfate to form. As the adsorbed layer of hydrated Ca-sulfate gets thicker, cracks form in the adsorbed layer enabling migration of H₂O and complete conversion of the anhydrite to gypsum. These experiments showed that gypsum formed progressively faster as the temperature was dropped from 40 to 20 to 10 °C (Sievert et al. 2005). Dry grinding of gypsum was found to produce some bassanite after only 15 min, but the reaction only continued completely in the presence of clay additives; 35 wt% talc was found to be the most effective agent tested (Zhang et al. 1996). Additives also influenced the morphology of gypsum crystals and the rate kinetics (Badens et al. 1999).

METHOD

The samples in this study were obtained from multiple sources (e.g., collected in North America, Europe, Africa, or synthesized in the lab) and are listed in Table 1. For sample JB1464 a gypsum rock was crushed and any dark grains were removed. The grains were gently ground in a mortar and pestle and dry sieved into several grain sizes. The 45–90 μm fraction was wet sieved with methanol in addition to remove fines. The ML-S6 gypsum sample was wet sieved at the time of preparation in 1993. The 63–90 μm (JB557) size fraction was rewashed in 2000 before reflectance spectra were measured. The <63 μm size fraction appears to have partially altered to bassanite by the time the reflectance spectra were run in 2000. Spectra were also measured for this study of gypsum samples JB1464a–e and the anhydrite sample JB641. The bassanite sample from the U.S. Geological Survey collection (Clark et al. 2007) is GDS145, formed by heating gypsum at 60 °C by Crowley (1991). One anhydrite sample (JB641, DD102) contains minor admixtures that contribute an iron band, but no hydration features, while another anhydrite sample (GDS42 from the USGS collection) (Clark et al. 2007) is slightly hydrated and contains a weak iron band.

Measurement of reflectance spectra

Reflectance spectra were measured for this study at Brown University's RELAB using a bidirectional VNIR spectrometer under ambient conditions relative to Halon and a biconical Nicolet Fourier transform infrared (FTIR) spectrometer in a controlled, dry environment relative to a rough gold surface as in previous studies (e.g., Bishop and Murad 2005). The bidirectional spectra were acquired from 0.3–2.5 μm at 5 nm spectral sampling. Infrared reflectance spectra were measured with 2 cm⁻¹ spectral sampling from 1–50 μm in an environment purged of H₂O- and CO₂- for 10–12 h.

Composite, absolute reflectance spectra were prepared by scaling the FTIR data to the bidirectional data near 1.2 μm.

Additional FTIR reflectance spectra were collected at the USGS Spectroscopy Laboratory (Clark et al. 2007), available online at <http://speclab.cr.usgs.gov/> and from Salisbury et al. (1991). The Salisbury spectral archive includes hemispherical reflectance spectra of grains <75, 75–250 μm, and mineral surfaces.

A continuum was removed from the spectra across the ranges 1.28–1.64, 2.05–2.35, and 3.8–5.0 μm of selected spectra to facilitate comparison of the band strengths as proposed in Brown (2006) and implemented in Brown et al. (2008).

Measurement of emission spectra

The emitted radiation from various mineral and rock samples was measured by Lane (2007) using a modified Nicolet Nexus 670 FTIR interferometric spectrometer over the range of 2000 to 200 cm⁻¹ with 2 cm⁻¹ spectral sampling. The gypsum samples were measured at ~50 °C and the others at ~80 °C. Two blackbody targets (at ~70 and 100 °C) were measured to determine the instrument response function and instrument temperature used for data calibration. The emission spectra of the minerals were obtained by reducing the raw wavelength and temperature-dependent data according to the one-temperature procedure of Ruff et al. (1997), assuming that sample emission equals unity at the Christiansen feature (e.g., Logan et al. 1975; Salisbury 1993).

Measurement of transmittance spectra

Transmittance spectra were measured by Salisbury et al. (1991) of one anhydrite and two gypsum samples by mixing the minerals with KBr to prepare pellets for analysis.

RESULTS

VNIR spectra

Hydrated Ca-sulfates exhibit a characteristic triplet near 1.4 μm and strong features near 1.9, 2.8–3.1, and 4.2–5 μm (Fig. 2). The triplet occurs at 1.446, 1.490, and 1.538 μm for gypsum and at 1.428, 1.476, and 1.540 μm for bassanite (Fig. 3; Table 2). Another triplet is observed in spectra of gypsum at 2.178, 2.217, and 2.268 μm; however, spectra of bassanite exhibit multiple weaker features here at 2.10, 2.164, 2.219, 2.262, and 2.268 μm (Fig. 4; Table 2). An additional band is observed at 2.268 μm in gypsum spectra and as a doublet at 2.262 and 2.268 μm in bassanite spectra. These are attributed to H₂O as well because they are not observed for anhydrite. Interestingly, the partially hydrated anhydrite spectrum has a shoulder feature here (Fig. 2).

Spectra of all Ca-sulfates exhibit multiple combination and overtone features near 4.2–5 μm (Fig. 5). Anhydrite spectra provide several distinct bands, whereas the spectra of bassanite and gypsum include broader features of overlapping bands. The anhydrite features occur at 4.203, 4.286, 4.348, 4.469, 4.668, 4.691, and 4.925 μm (Table 2). Besides the overlap-broadened

TABLE 1. Summary of spectral features for Ca-sulfates

Mineral	Location	Grain size (μm)	Sample ID no.	Reference
gypsum	Niedersachswerfen, Nordhausen, Harz, Germany	<45, 45–90, 90–125, 125–250, >250	JB1464	this study, from Gunnar Farber Mineralien
gypsum ^a /bassanite	Mule Canyon, California	<63	ML-S6, JB556	Lane and Christensen (1998)
gypsum	Mule Canyon, California	63–90	ML-S6, JB557	Lane and Christensen (1998)
gypsum	Eddy County, New Mexico	rock surface	ML-S8	Lane and Christensen (1998)
gypsum	Italy	<75, 75–250, rock surface, KBr pellet	26B	Hunt et al. (1971); Salisbury et al. (1991)
gypsum	Vermont	<75, 75–250, rock surface, KBr pellet	333B	Hunt et al. (1971); Salisbury et al. (1991)
bassanite	synthetic	50–1000	GDS145	Crowley et al. (1991); Clark et al. (2007)
bassanite		rock surface	ML-S11	Lane and Christensen (1998)
anhydrite	Djebel Melah d'El Outaya, Massif de l'Aures, Biskra, Hautes Plateau, Algeria	rock surface	JB641, DD102	this study, from mineral dealer
anhydrite	Carson City, Nevada	rock surface	ML-S16	Lane and Christensen (1998)
anhydrite	France	<75, 75–250, rock surface, KBr pellet	NMNH46393	Salisbury et al. (1991)
anhydrite	New Mexico	<250 (avg ~150)	GDS42	Clark et al. (2007)

^a Sample ML-S6 was gypsum at the time emission spectra were obtained, but had partially altered to bassanite by the time the reflectance spectra were acquired.

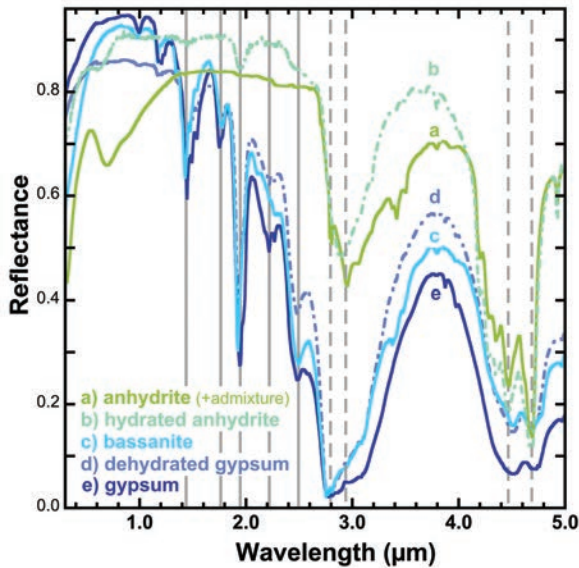


FIGURE 2. VNIR reflectance spectra from 0.35 to 5.0 mm of selected Ca-sulfates measured in a dry environment: fine-grained anhydrite from Algeria, fine-grained anhydrite from France, bassanite synthesized from gypsum, altered (dehydrated) gypsum, and gypsum. The gray lines mark bands and facilitate observation of differences in the spectral features of gypsum, bassanite, and anhydrite. (Color online.)

features in this region, the distinguishing feature of gypsum and bassanite spectra compared to anhydrite spectra is a shift of the band at 4.925 to ~4.97 μm for bassanite and gypsum.

Mid-IR spectra

The strongest mid-IR bands are due to SO₄ ν₃ and ν₄ vibrations (Figs. 6–7). Additional deep bands are seen in the emission data that result from metal-oxygen or lattice modes (Lane 2007). The ν₃ vibration is observed as a doublet or triplet near 1150–1200 cm⁻¹ (Table 2) and the ν₄ vibration is observed as a doublet or triplet near 600–690 cm⁻¹. The nature of these bands depends on grain size with finer-grained samples exhibiting shoulders and additional spectral character in the region between the fundamental bands, as well as a weakening of the fundamental bands (Lane and Christensen 1998). Transmittance spectra exhibit sharp triplets for both ν₃ and ν₄ (Fig. 8; Ross 1974; Salisbury et al. 1991). These triplets are also seen in the transmission spectra of bassanite and anhydrite of Moenke (1962). However, in the gypsum spectrum of Moenke (1962), ν₃ and ν₄ are represented by doublets, but these doublets have spectral character (i.e., a band broadening) that indicates a third band for both the ν₃ and ν₄, but these third bands are largely degenerate.

The ν₁ vibration is observed as an absorption band at 1015, 1012, and 1005 cm⁻¹, respectively, for anhydrite, bassanite, and gypsum in reflectance spectra (Figs. 6–7) and is stronger for fine-grained samples. Transmittance spectra of anhydrite and gypsum also have a weak to very weak ν₁ feature (Fig. 8; Ross 1974; Moenke 1962). The bassanite transmission spectrum of Moenke (1962) shows the ν₁ feature to be much stronger and more apparent.

The ν₂ vibration is seen at 510 cm⁻¹ in reflectance/emis-

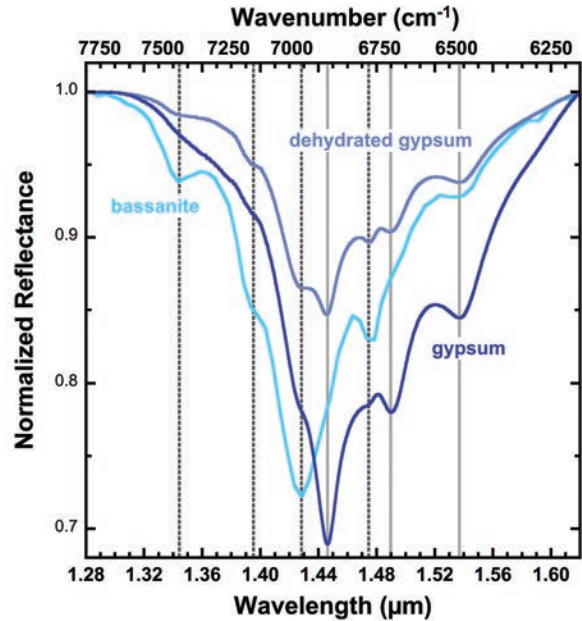


FIGURE 3. Continuum-removed spectra of hydrated Ca-sulfates across the 1.28–1.6 mm region. (Color online.)

TABLE 2. Summary of spectral features for Ca-sulfates

	Anhydrite Ca(SO ₄)	Bassanite Ca(SO ₄)·0.5H ₂ O	Gypsum Ca(SO ₄)·2H ₂ O
NIR bands in μm (and cm⁻¹)			
H ₂ O		1.344 (7440)	
combinations and overtones		1.428, 1.476, 1.54 (7003, 6775, 6494)	1.446, 1.490, 1.538 (6916, 6711, 6502)
		1.78 (5618)	1.750 (5714)
		1.93 (5181)	1.942 (5149)
		2.10 (4762)	
		2.164 (4621)	2.178 (4591)
		2.219 (4507)	2.217 (4511)
		2.262, 2.268 (4421, 4409)	2.268 (4409)
		2.484 (4026)	2.486 (4023)
H ₂ O stretch	~2.9 (~3450)	2.75–3.1 (~3640–3230)	2.75–3.1 (~3640–3230)
SO ₄	3.924 (2548)	3.871, 3.968, 4.004 (2583, 2520, 2498)	3.871, 3.975 (2583, 2516)
combinations and overtones	4.203, 4.286, 4.348 (2379, 2333, 2300)		
		4.506 (2219)	4.487 (2229)
	4.668, 4.691 (2142, 2132)	4.688 (2142)	4.689 (2133)
	4.925 (2030)	4.966 (2014)	4.972 (2011)
mid-IR peaks in cm⁻¹ (and μm)			
↓ H ₂ O bend	1693 (5.91)	1684 (5.94)	1681 (5.95)
↓ H ₂ O bend	1623 (6.16)	1628 (6.14)	1630 (6.13)
↓ H ₂ O bend	1545 ^a (6.47)	~1500 ^a (6.67)	~1530 ^a (6.54)
↑ SO ₄ ν ₃	1197, 1156 (8.35, 8.65)	1169, 1157 (8.55, 8.64)	1195, 1154 (8.37, 8.67)
↓ SO ₄ ν ₁	1015 ^a (9.85)	1012 ^a (9.88)	1005 ^a (9.95)
↑ SO ₄ ν ₄	687 (14.6)	663 (15.1)	673 (14.9)
↑ SO ₄ ν ₄	619, 597 (16.2, 16.8)	598 (16.7)	604 (16.6)
↓ SO ₄ ν ₂	510 ^a (19.6)	~490 (20.4)	~470 (21.3)
↑	266 (37.6)	240, 225 (41.7, 44.4)	

Notes: Arrows indicate if the feature is present as an absorption (down) or a peak (up). ^a Band is present for fine-grained samples.

sion spectra of fine-grained anhydrite, but is difficult to detect in spectra of coarse-grained samples or surfaces (Figs. 6–9). Transmittance spectra of anhydrite show this feature at 515 cm⁻¹ (Fig. 8; Ross 1974; Moenke 1962). The broader, weaker ν₂ bands

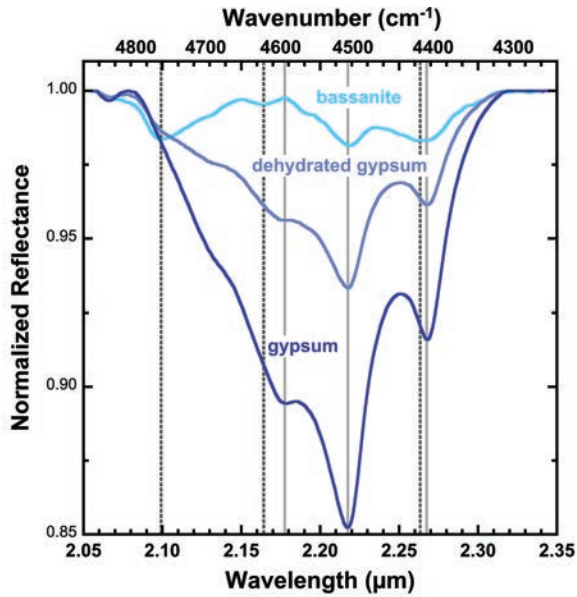


FIGURE 4. Continuum-removed spectra of several Ca-sulfates across the 2.05–2.35 mm region. (Color online.)

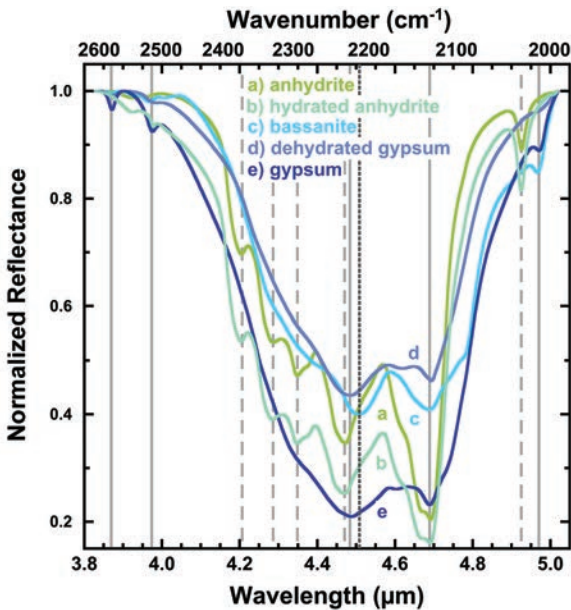


FIGURE 5. Continuum-removed spectra of several Ca-sulfates across the 3.8–5.0 mm region. (Color online.)

occur at lower frequencies in reflectance and emission spectra (Figs. 6–7) and as doublets at lower frequencies for bassanite and gypsum in transmittance spectra (Ross 1974).

Additional weak bands are observed at 843, 894, and 1543 cm^{-1} for reflectance spectra of fine-grained anhydrite (Figs. 6 and 9), but are not found in transmittance spectra or in reflectance/emission spectra of the coarse-grained samples or the mineral surfaces.

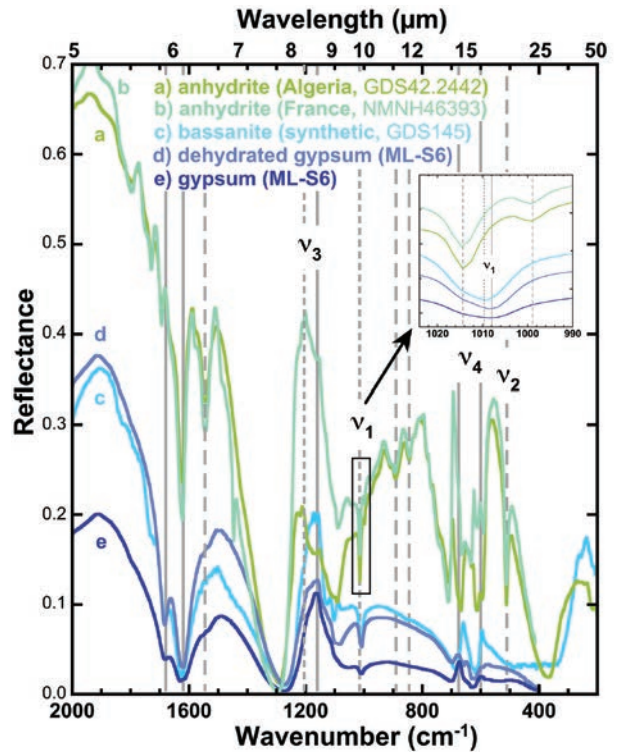


FIGURE 6. Mid-IR reflectance spectra of several Ca-sulfates: fine-grained anhydrite from Algeria, fine-grained anhydrite from France (Salisbury et al. 1991), bassanite synthesized from gypsum, dehydrated gypsum, and gypsum (Lane 2007). (Color online.)

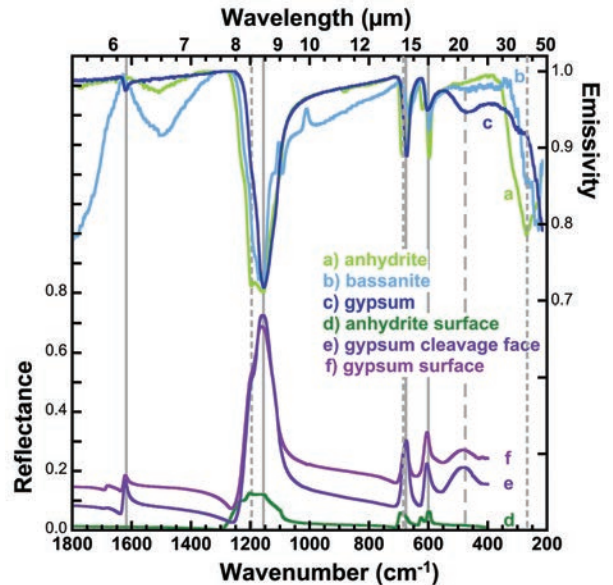


FIGURE 7. Mid-IR spectra of several Ca-sulfates including emission spectra from Lane (2007): (a) anhydrite, (b) fine-grained bassanite, and (c) gypsum, and hemispherical reflectance spectra from Salisbury et al. (1991): (d) an anhydrite sample from France, (e) a gypsum cleavage face from Vermont, and (f) a gypsum sawn surface from Italy. (Color online.)

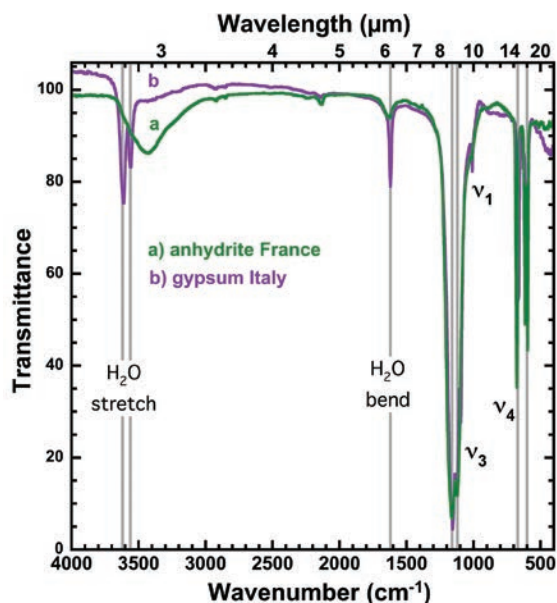


FIGURE 8. Mid-IR transmittance spectra of anhydrite and gypsum Salisbury et al. (1991). (Color online.)

Effects of grain size and relative humidity

The effects of grain size are shown in the mid-IR region for gypsum in Figure 10, where the v_3 and v_4 modes increase in intensity with increasing grain size. The v_2 mode remains about the same for most spectra, but is not observed in the spectrum of the finest size fraction, while the v_1 mode becomes more obvious with decreasing grain size (Fig. 10; Lane and Christensen 1998). Additional $\delta\text{H}_2\text{O}$ bands near 1600–1700 cm^{-1} increase in intensity, and lattice modes near 150–250 cm^{-1} decrease in intensity with decreasing grain size. The emission and biconical reflectance spectra of the >250 μm gypsum are similar; however, the shape of the v_3 triplet near 1150–1200 cm^{-1} differs.

The effects of grain size on the VNIR spectra of gypsum are shown in Figure 11. The spectral brightness and band depth for all features increases with decreasing grain size. The VNIR bands are dependent on relative humidity as well as grain size. Spectra of three size fractions are shown in Figure 12 that were measured under ambient and dehydrated conditions (air purged of H_2O and CO_2). A systematic trend can be seen for increasing band depth for the H_2O features in the spectra measured under ambient conditions compared to those measured under H_2O -purged conditions.

DISCUSSION

v_3 vibrations

The dominant v_3 vibrations for anhydrite occur at 1121 and 1159 cm^{-1} in the transmittance spectra of Salisbury et al. (1991; Fig. 9), at 1095, 1126, and 1149 cm^{-1} in the Ross (1974) data and at 1130 and 1159 cm^{-1} in the Moenke (1962) data. They occur instead at 1155, 1167, and 1201 cm^{-1} in reflectance data of an anhydrite surface (Fig. 9; Salisbury et al. 1991) and at 1158 and 1200 cm^{-1} in emission data of an anhydrite surface (Fig. 7; Lane 2007). A shoulder near 1240 cm^{-1} in the reflectance spectrum of

the anhydrite surface becomes stronger for the spectrum of the 75–250 μm size fraction of anhydrite. For the <75 μm anhydrite reflectance spectrum the v_3 vibration is a doublet with the strongest peak at 1236 cm^{-1} and another peak at 1213 cm^{-1} and a shoulder at 1154 cm^{-1} . The v_3 Raman triplet bands occur at 1124 and 1157 cm^{-1} for anhydrite (Prasad et al. 2005).

The v_3 vibrations in bassanite spectra exhibit more character than in the spectra of gypsum or anhydrite. They are observed at 1100, 1120, and 1158 cm^{-1} with a shoulder near 1180 cm^{-1} in transmittance spectra (Moenke 1962) and at 1096, 1116, 1153, and 1168 cm^{-1} in Raman spectra (Prasad et al. 2005), whereas they occur at 1090, 1117, 1157, and 1172 cm^{-1} with a shoulder near 1200 cm^{-1} in reflectance data (Fig. 6), and at 1092, 1122, and 1157 cm^{-1} with a shoulder near 1185 cm^{-1} in emission data (Fig. 7, Lane 2007).

Gypsum exhibits a similar trend for the v_3 vibrations (Fig. 9, Salisbury et al. 1991) with transmittance bands at 1096, 1130, and 1155 cm^{-1} (Fig. 9) in the Salisbury et al. (1991) data, as a triplet at 1117, 1138, and 1144 cm^{-1} or 1118, 1131, and 1142 cm^{-1} in the Ross (1974) data, and as a doublet at 1120 and 1150 cm^{-1} with a shoulder at higher wavenumbers in the Moenke (1962) data. A

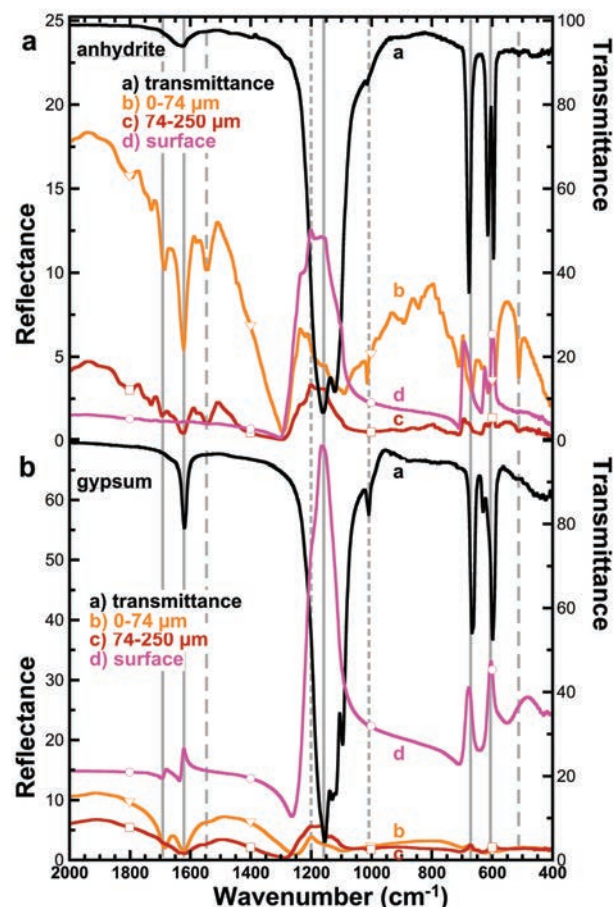


FIGURE 9. Mid-IR reflectance and transmittance spectra of (a) anhydrite from France and (b) gypsum from Italy (data from Salisbury et al. 1991). The reflectance spectra include a fracture surface for the anhydrite and a sawn surface for the gypsum. (Color online.)

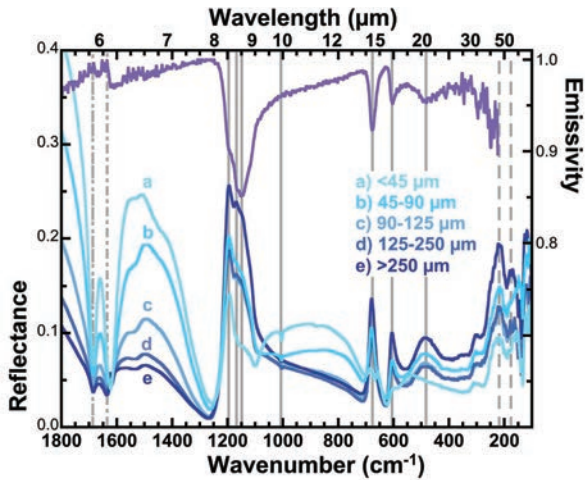


FIGURE 10. Mid-IR reflectance spectra from 100–1800 cm^{-1} of multiple grain size fractions of gypsum and emission spectra of the >250 μm size fraction. (Color online.)

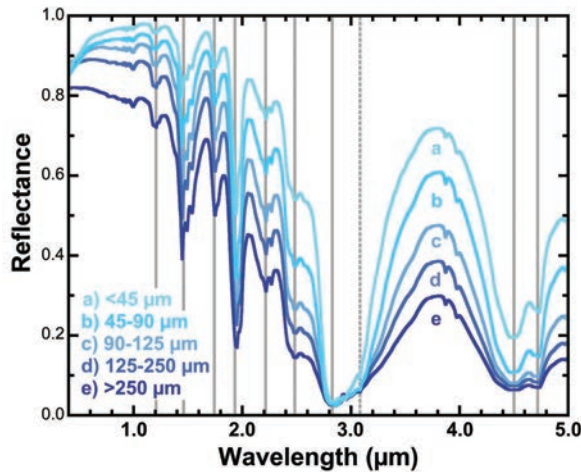


FIGURE 11. VNIR reflectance spectra from 0.4–5 μm of multiple grain size fractions of gypsum. (Color online.)

triplet is observed at 1117, 1145, and 1167 cm^{-1} for the ν_3 vibrations in Raman spectra of gypsum (Prasad et al. 2005). Gypsum surface spectra exhibit a band at 1165 cm^{-1} with a shoulder near 1200 cm^{-1} in reflectance data (Fig. 9, Salisbury et al. 1991) and a band at 1154 cm^{-1} with a shoulder near 1200 cm^{-1} in emission data (Fig. 7; Lane 2007). The ν_3 vibration becomes a peak at 1200 cm^{-1} in reflectance spectra of the fine-grained samples (Figs. 9b and 10).

Differences are observed between transmittance spectra peak positions and reflectance/emission spectra peak positions because transmittance spectra depend only on the absorption properties, whereas reflectance and emission spectra are a function of both the real, n , and imaginary, k , indices of refraction (e.g., Logan et al. 1975; Hapke 1981; McMillan and Hofmeister 1988). Reflectance and emission spectra in the mid-IR region are dominated by surface scattering for coarse-grained materials or surfaces resulting in strong reststrahlen bands and by volume scattering

for fine particles resulting in weaker reststrahlen bands and strong transparency features (Salisbury and Wald 1992; Mustard and Hays 1997; Lane 1999; Bishop et al. 2004). For this reason reflectance and emission spectra also vary with grain size. For materials like Ca-sulfates where the refractive index is ~ 1.5 some of the mid-IR vibrational features invert from bands to peaks (i.e., the ν_3 mode at 1110 cm^{-1} in Figs. 9–10). Other minerals have higher indices of refraction and do not exhibit this trend (Dyar et al. 2008). The inversion from bands to peaks with grain size is also observed for mid-IR spectra of calcite (Salisbury and Wald 1992; Lane and Christensen 1998; Lane 1999), which has a refractive index ~ 1.5 (Dyar et al. 2008). Reflectance (R) and emission (E) spectra are related by Kirchhoff's Law, $E = 1 - R$, which generally holds for hemispherical or off-axis reflectance spectra, but does not always work for smaller grains (Hunt and Vincent 1968; Salisbury and Wald 1992; Hapke 1993; Wenrich and Christensen 1996).

ν_1 vibrations

The ν_1 vibration occurs as a single band in spectra of Ca-sulfates and follows a similar trend for transmittance, Raman, reflectance, and emission spectra, where the vibrational energy shifts toward lower frequencies as the mineral becomes hydrated. The ν_1 band is observed at 1013, 1012, and 1006 cm^{-1} in transmittance spectra of anhydrite, bassanite, and gypsum, respectively (Moenke 1962; Ross 1974), and is observed at 1014, 1008, and 1005 cm^{-1} in Raman spectra of anhydrite, bassanite, and gypsum, respectively (Prasad et al. 2005). This feature is observed at 1015, 1012, and 1005 cm^{-1} , respectively, in reflectance spectra for fine-grained samples (Fig. 6).

ν_4 vibrations

The ν_4 vibrations for anhydrite occur as a triplet at 596, 615, and 677 cm^{-1} in the transmittance spectra of Salisbury et al. (1991; Fig. 9), at 592, 612, and 671 cm^{-1} in the Ross (1974) data and at 597, 616, and 676 cm^{-1} in the Moenke (1962) data. Raman vibrations for the anhydrite ν_4 mode are observed at 595, 615, and 676 cm^{-1} (Prasad et al. 2001). Reststrahlen peaks are observed at 597,

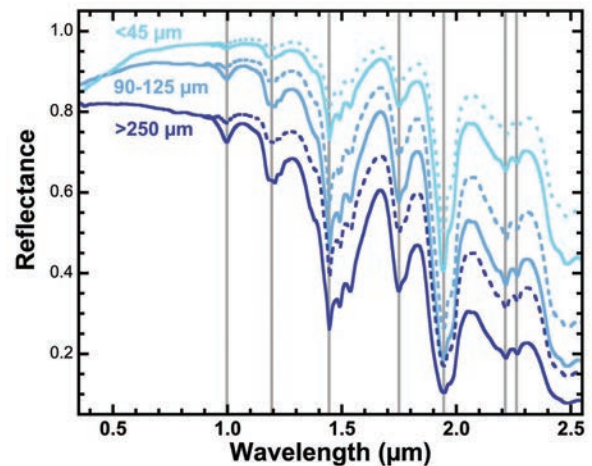


FIGURE 12. VNIR reflectance spectra from 0.35–2.55 μm of three grain size fractions of gypsum measured under ambient (solid line) and dehydrated (dashed line) moisture conditions. (Color online.)

619, and 687 cm^{-1} in reflectance spectra of an anhydrite surface (Fig. 9; Salisbury et al. 1991) and bands are found at 596, 619, and 687 cm^{-1} in emission data (Fig. 7; Lane 2007). As the grain size decreases, the ν_4 vibrations invert and become absorptions instead of peaks. These are observed at 592, 613, and 669 cm^{-1} (i.e., spectra b vs. d in Fig. 9).

Transmittance spectra of bassanite have a triplet for the ν_4 mode that is observed at 605, 634, and 667 cm^{-1} (Moenke 1962; Ross 1974) and Raman spectra of bassanite have a doublet at 601 and 660 cm^{-1} (Prasad et al. 2005). The bassanite ν_4 bands occur at 596 and 660 cm^{-1} in reflectance spectra (Fig. 6) and at 598 and 663 cm^{-1} in emission spectra (Fig. 7; Lane 2007).

Gypsum spectra exhibit a doublet for the ν_4 mode that is observed in the transmittance data of Salisbury et al. (1991; Fig. 9) at 598 and 666 cm^{-1} , in the Ross (1974) data near 603 and 674 cm^{-1} or 622 and 669 cm^{-1} , and in the Moenke (1962) data at 605 and 673 cm^{-1} . The ν_4 vibrations occur at 602 and 669 cm^{-1} in Raman spectra of gypsum (Prasad et al. 2005). Gypsum surface spectra exhibit a doublet at 604 and 678 cm^{-1} in reflectance data (Fig. 9; Salisbury et al. 1991) and bands at 604 and 677 cm^{-1} in emission data (Fig. 7; Lane 2007). Gypsum's ν_4 vibrations start to flip in reflectance spectra of the fine-grained samples and exhibit multiple weak up and down features or peak reversals from 586–700 cm^{-1} (Figs. 9–10).

ν_2 vibrations

The ν_2 vibration occurs as a very weak single band at 515 cm^{-1} in transmittance spectra of anhydrite (Fig. 9; Moenke 1962; Ross 1974; Salisbury et al. 1991), while two bands at 424 and 490 cm^{-1} are observed for the ν_2 vibration in Raman spectra of anhydrite (Prasad et al. 2001), and a single band is observed in fine-grained spectra of anhydrite, but not in surface spectra of anhydrite (Fig. 9a).

Two broad, weak bands are observed near 420 and 465 cm^{-1} in transmittance spectra for the ν_2 vibration of bassanite (Moenke 1962), while two bands at 421 and 490 cm^{-1} are observed for the ν_2 vibration in Raman spectra of gypsum (Prasad et al. 2001). No bands were observed for the ν_2 vibration in reflectance and emission spectra of bassanite in our study.

A broad, weak band from about 415–490 cm^{-1} is observed in transmittance spectra for the ν_2 vibration of gypsum (Fig. 9; Moenke 1962; Ross 1974; Salisbury et al. 1991), while two bands at 420 and 494 cm^{-1} are observed for the ν_2 vibration in Raman spectra of gypsum (Prasad et al. 2001), and a weak, broad band is observed near 480 cm^{-1} in reflectance spectra and near 460 cm^{-1} in emission spectra of gypsum (Fig. 7).

Characteristic features of Ca-sulfates

Gypsum and bassanite exhibit characteristic bands near 1.4–1.5, 1.93–1.94, and 2.1–2.3 μm due to H_2O vibrations and additional mostly broad bands from 4.2–5 μm due to SO_4 vibrations. Anhydrite spectra contain multiple individual bands from 4.2–5 μm due to SO_4 vibrations. The mid-IR region spectra exhibit strong $\text{SO}_4 \nu_3$ vibrational bands near 1150–1200 cm^{-1} and ν_4 vibrational bands near 600–680 cm^{-1} . Additional weaker features are observed near 1005–1015 cm^{-1} for the ν_1 mode and near 470–510 cm^{-1} for the ν_2 mode. The mid-IR H_2O bending vibration occurs near 1623–1630 cm^{-1} . The visible/near-infrared region spectra are

brighter and have deeper bands for the finer-grained samples. In the mid-IR region the ν_4 absorptions transition to peaks in spectra of the finer-grained samples, the ν_1 vibration occurs as an absorption instead of a peak and has the strongest intensity in spectra of the finer-grained samples. The ν_2 vibration is a sharp band for anhydrite and a broad peak for gypsum. The band center of the ν_1 vibration follows a trend of decreasing frequency (increasing wavelength) with increasing hydration of the sample in the transmittance, Raman, and reflectance spectra. The ν_2 vibration tends to follow this trend as well.

IMPLICATIONS FOR MARS

The largest gypsum deposit on Mars is present at the north polar sand dunes of the Olympia Undae region (Langevin et al. 2005; Fishbaugh et al. 2007). Fishbaugh et al. (2007) hypothesized that the gypsum in the dunes formed by water emanating from nearby channels, whereas Masse et al. (2012) proposed the gypsum grains formed by weathering of dust particles. Szumila et al. (2013) found that gypsum has a higher abundance in primary dunes at Olympia Undae rather than secondary dunes that formed subsequently, indicating that gypsum was likely present when the dunes formed and may be altering under current conditions. No evidence was observed for changes in the form of the Ca-sulfate due to modification of the dunes (Szumila et al. 2013).

Gypsum is also thought to be present in small veins observed in rocks at Endeavor Crater by the Opportunity rover (Squyres 2012). These are interpreted to have formed as water flowed through cracks in the rocks that later became exposed at the surface as the rocks were eroded (Squyres 2012). Gypsum has also been found in some rocks and soils of the Columbia Hills in Gusev Crater (Squyres et al. 2006; Yen et al. 2008). If a NIR spectrometer is sent to Mars on a future rover then the characteristic features near 1.4–1.5, 1.93–1.94, and 2.1–2.3 μm could be used to determine if gypsum or bassanite were present in rocks or veins like these observed at Endeavor Crater and the Columbia Hills. Discovering this would provide constraints on the temperature and pH of the formation environment as gypsum generally forms below 40 $^{\circ}\text{C}$ at neutral pH and bassanite typically forms at temperatures above 120 $^{\circ}\text{C}$ and at pH 8–9.

Wray et al. (2011) used CRISM spectra to identify gypsum associated with Fe/Mg-sulfates in a discreet ring around the walls of Columbus Crater, whereas Weitz et al. (2014) found Ca-sulfate in outcrops along the western Melas Chasma floor and Weitz et al. (2013) identified gypsum outcrops in a trough at Noctis Labyrinthus. Mangold et al. (2010) observed Ca-sulfate in a separate Noctis Labyrinthus trough farther to the east and suggested that local frost/snow reacted with Ca and S to form gypsum due to lack of evidence for evaporative processes. Weitz et al. (2013) suggest that if hydrothermal conditions existed that enabled snow and ice to melt, then the associated heat would also allow gypsum to precipitate. As gypsum formation is favored over other Ca-sulfates at temperatures below $\sim 40^{\circ}\text{C}$, temperatures were likely not elevated much above this if hydrothermal processes took place.

Wray et al. (2010) observed bassanite in the floor of the outflow channel at Mawrth Vallis. The bassanite was found in topographic lows surrounded by exposures of Fe/Mg-smectites and the bassanite appears to have been emplaced prior to the clay-rich unit. This is contrary to the more commonly observed

sequence of phyllosilicates in Noachian terrains and sulfates in younger Hesperian terrains (Bibring et al. 2006). Baldrige et al. (2009) reported fieldwork on sulfates from dry lakes in the Western Australian playa regions and suggested that sulfate deposition could take place contemporaneously with phyllosilicate deposition within natural terrestrial settings. This work was guided by maps of sulfate in the dry lakes created from ASTER satellite data (Brown and Cudahy 2006). Spectra of bright units at Mawrth Vallis (e.g., Wray et al. 2010; Bishop et al. 2013) are not consistent with the presence of gypsum, although it is unknown if anhydrite is present. This indicates that the relative humidity is sufficiently low for the Ca-sulfate to remain in the bassanite state. Possibly the Ca-sulfate observed at Mawrth Vallis is fine grained and more readily dehydrated to bassanite than in other locations such as the gypsum-bearing sand dunes at Olympia Undae. The clays at Mawrth Vallis may have also facilitated bassanite formation from gypsum through wind abrasion, as clays are an industrial additive for gypsum conversion to bassanite through grinding.

Spectral data presented here will enable more detailed identification of Ca-sulfates on Mars and may allow for grain size determinations in some outcrops. The variable temperature, pH, and salt concentration regimes that govern which Ca-sulfate mineral forms can thus be used to provide constraints on the geochemical environment of Ca-sulfate outcrops on Mars using orbital and rover spectroscopy.

ACKNOWLEDGMENTS

We are grateful for support from NASA's Mars Fundamental Research Program Grant NNX11AF116. We also thank T. Hiroi at Brown University's RELAB for measuring many of the reflectance spectra used in the study and the PGGURP program for providing support for S. King. Thoughtful comments from Karly Pitman and an anonymous reviewer greatly improved the manuscript. Any use of trade, firm, or product names is for descriptive purposes only and does not imply endorsement by the U.S. Government. This work is PSI Contribution Number 607.

REFERENCES CITED

- Allen, R.D., and Kramer, H. (1953) Occurrence of bassanite in two desert basins in southeastern California. *American Mineralogist*, 38, 1266–1268.
- Appleyard, F.C. (1983) Gypsum and anhydrite—Industrial Minerals and Rocks (Nonmetallics Other than Fuels), 775–792. American Institute of Mining, Metallurgical, and Petroleum Engineers, New York.
- Badens, E., Veessler, S., and Boistelle, R. (1999) Crystallization of gypsum from hemihydrate in presence of additives. *Journal of Crystal Growth*, 198–199, 704–709.
- Baldrige, A.M., Hook, S.J., Crowley, J.K., Marion, G.M., Kargel, J.S., Michalski, J.L., Thomson, B.J., de Souza Filho, C.R., Bridges, N.T., and Brown, A.J. (2009) Contemporaneous deposition of phyllosilicates and sulfates: Using Australian acidic saline lake deposits to describe geochemical variability on Mars. *Geophysical Research Letters*, 36, 1–6.
- Belousov, A.B. (1995) The Shiveluch volcanic eruption of 12 November 1964—Explosive eruption provoked by failure of the edifice. *Journal of Volcanology and Geothermal Research*, 66, 357–365.
- Berenblut, B.J., Dawson, P., and Wilkinson, G.R. (1973) A comparison of the Raman spectra of anhydrite (CaSO₄) and gypsum (CaSO₄·2H₂O). *Spectrochimica Acta Part A: Molecular Spectroscopy*, 29, 29–36.
- Bibring, J.-P., Langevin, Y., Gendrin, A., Gondet, B., Poulet, F., Berthé, M., Soufflot, A., Arvidson, R., Mangold, N., Mustard, J., and Drossart, P. (2005) Mars surface diversity as revealed by the OMEGA/Mars Express observations. *Science*, 307, 1576–1581.
- Billo, S.M. (1987) Petrology and kinetics of gypsum-anhydrite transitions. *Journal of Petroleum Geology*, 10, 73–85.
- Bishop, J.L., and Murad, E. (1996) Schwertmannite on Mars? Spectroscopic analyses of schwertmannite, its relationship to other ferric minerals, and its possible presence in the surface material on Mars. In M.D. Dyar, C. McCammon, and M.W. Schaefer, Eds., *Mineral Spectroscopy: A Tribute to Roger G. Burns*, Special Publication Number 5, 337–358. The Geochemical Society, Houston, Texas.
- (2005) The visible and infrared spectral properties of jarosite and alunite. *American Mineralogist*, 90, 1100–1107.
- Bishop, J.L., Murad, E., Lane, M.D., and Mancinelli, R.L. (2004) Multiple techniques for mineral identification on Mars: A study of hydrothermal rocks as potential analogs for astrobiology sites on Mars. *Icarus*, 169, 331–333.
- Bishop, J.L., Loizeau D., McKeown N.K., Saper L., Dyar M.D., Des Marais D., Parente M., and Murchie S.L. (2013) What the ancient phyllosilicates at Mawrth Vallis can tell us about possible habitability on early Mars. *Planetary and Space Science*, 86, 130–149.
- Blaney, D.L., and McCord, T.B. (1995) Indications of sulfate minerals in the Martian soil from Earth-based spectroscopy. *Journal of Geophysical Research*, 100, 14433–14441.
- Bromehead, C.E.N. (1943) The forgotten uses of selenite. *Mineralogical Magazine*, 182, 325–333.
- Brown, A.J. (2006) Spectral curve fitting for automatic hyperspectral data analysis. *IEEE Transactions on Geoscience and Remote Sensing*, 44, 1601–1608.
- Brown, A.J., and Cudahy T.J. (2006) Hyperspectral imaging of sulfate evaporite deposits in Western Australia and on Mars. *SPIE Electronic Imaging*, San Jose, California.
- Brown, A.J., Sutter, B., and Dunagan, S. (2008) The MARTE imaging spectrometer experiment: Design and analysis. *Astrobiology*, 8, 1001–1011.
- Bundy, W.M. (1956) Petrology of gypsum-anhydrite deposits in southwestern Indiana. *Journal of Sedimentary Petrology*, 26, 240–252.
- Christensen, P.R., Bandfield, J.L., Hamilton, V.E., Ruff, S.W., Kieffer, H.H., Titus, T.N., Malin, M.C., Morris, R.V., Lane, M.D., Clark, R.L., and others. (2001) Mars Global Surveyor Thermal Emission Spectrometer experiment: Investigation description and surface science results. *Journal of Geophysical Research*, 106, 23823–23871.
- Clark, R.N., King, T.V.V., Klejwa, M., and Swayze, G.A. (1990) High spectral resolution reflectance spectroscopy of minerals. *Journal of Geophysical Research*, 95, 12653–12680.
- Clark, R.N., Swayze, G.A., Wise, R., Livo, E., Hoefen, T., Kokaly, R., and Sutley, S.J. (2007) USGS digital spectral library splib06a, Digital Data Series 231. U.S. Geological Survey.
- Cloutis, E.A., Hawthorne, F.C., Mertzman, S.A., Krenn, K., Craig, M.A., Marcino, D., Methot, M., Strong, J., Mustard, J.F., Blaney, D.L., Bell, J.F. III, and Vilas, F. (2006) Detection and discrimination of sulfate minerals using reflectance spectroscopy. *Icarus*, 184, 121–157.
- Conley, R.F., and Bundy, W.M. (1958) Mechanism of gypsification. *Geochimica et Cosmochimica Acta*, 15, 57–72.
- Crowley, J.K. (1991) Visible and near-infrared (0.4–2.5 μm) reflectance spectra of Playa evaporite minerals. *Journal of Geophysical Research: Solid Earth*, 96, 16231–16240.
- Deer, W.A., Howie R.A., and Zussman J. (1992) *An Introduction to the Rock-Forming Minerals*, 528 p. Longman, London.
- Dyar, M.D., Gunter M.E., and Tasa D. (2008) *Mineralogy and Optical Mineralogy*, 708 p. Mineralogical Society of America, Chantilly, Virginia.
- Fenton, L.K., Bishop, J.L., Lafuente, B., Horgan, B.H., Szykiewicz, A., Bustos, D., and King, S.J. (2014) Preliminary results from a field study of the mineralogy of White Sands National Monument Dune Field. *Lunar and Planetary Science Conference XLV, The Woodlands, Texas*, Abstract 2855.
- Fishbaugh, K.E., Poulet, F., Chevrier, V., Langevin, Y., and Bibring, J.-P. (2007) On the origin of gypsum in the Mars north polar region. *Journal of Geophysical Research*, 112, E07002.
- Grotzinger, J.P., Arvidson, R.E., Bell, J.F. III, Calvin, W.M., Clark, B.C., Fike, D.A., Golombek, M., Greeley, R., Haldemann, A., Herkenhoff, K.E., and others. (2005) Stratigraphy and sedimentology of a dry to wet eolian depositional system, Burns formation, Meridiani Planum, Mars. *Earth and Planetary Science Letters*, 240, 11–72.
- Gunatillaka, A., Al-Temeemi, A., Saleh A., and Nassar, N. (1985) A new occurrence of bassanite in recent evaporitic environments, Kuwait, Arabian Gulf. *Journal of the University of Kuwait (Science)*, 12, 157–166.
- Hapke, B. (1981) Bidirectional reflectance spectroscopy, 1. Theory. *Journal of Geophysical Research*, 86, 3039–3054.
- (1993) Combined theory of reflectance and emittance spectroscopy. In C.M. Pieters and P.A.J. Englert, Eds., *Remote Geochemical Analysis: Elemental and Mineralogical Composition*, p. 31–42. Cambridge University Press, U.K.
- Hardie, L.A. (1967) The gypsum-anhydrite equilibrium at one atmosphere pressure. *American Mineralogist*, 52, 171–200.
- Hardie, L.A., and Eugster, H.P. (1971) The depositional environment of marine evaporites: A case for shallow, clastic accumulation. *Sedimentology*, 16, 187–220.
- Harrison, T.N. (2012) Experimental VNIR reflectance spectroscopy of gypsum dehydration: Investigating the gypsum to bassanite transition. *American Mineralogist*, 97, 598–609.
- Hawthorne, F.C., Krivovichev S.V., and Burns P.C. (2000) The crystal chemistry of sulfate minerals. In C.N. Alpers, J.L. Jambor, and D.K. Nordstrom, Eds., *Sulfate Minerals: Crystallography, Geochemistry, and Environmental Significance*. Reviews in Mineralogy and Geochemistry, 40, 1–112.
- Haynes, S.J., Boland, R., and Hughes-Pearl, J. (1989) Depositional setting of gypsum deposits, southwestern Ontario; the Domtar Mine. *Economic Geology*, 84, 857–870.

- Holland, H.D. (2002) Volcanic gases, black smokers, and the great oxidation event. *Geochimica et Cosmochimica Acta*, 66, 3811–3826.
- Hunt, G.R., and Vincent, R.K. (1968) The behavior of spectral features in the infrared emission from particulate surfaces of various grain sizes. *Journal of Geophysical Research*, 73, 6039–6046.
- Hunt, G.R., Salisbury, J.W., and Lenhoff, C.J. (1971) Visible and near-infrared spectra of minerals and rocks: IV. Sulphides and sulphates. *Modern Geology*, 3, 1–14.
- Innorta, G., Rabbi, E., and Tomadin, L. (1980) The gypsum-anhydrite equilibrium by solubility measurements. *Geochimica et Cosmochimica Acta*, 44, 1931–1936.
- Kushnir, J. (1982) The partitioning of seawater cations during the transformation of gypsum to anhydrite. *Geochimica et Cosmochimica Acta*, 46, 433–446.
- Lafuente, B., Bishop, J.L., Fenton, L.K., King, S.J., Blake, D., Sarrazin, P., Downs, R.T., Horgan, B.H., and Garcia, G.C. (2014) Mineralogical characterization by XRD of gypsum dunes at White Sands National Monument and application to gypsum detection on Mars. Lunar and Planetary Science Conference XLV, The Woodlands, Texas, Abstract 2284.
- Lane, M.D. (1999) Midinfrared optical constants of calcite and their relationship to particle size effects in thermal emission spectra of granular calcite. *Journal of Geophysical Research*, 104, 14099–14108.
- (2007) Mid-infrared emission spectroscopy of sulfate and sulfate-bearing minerals. *American Mineralogist*, 92, 1–18.
- Lane, M.D., and Christensen, P.R. (1998) Thermal infrared emission spectroscopy of salt minerals predicted for Mars. *Icarus*, 135, 528–536.
- Langevin, Y., Poulet, F., Bibring, J.-P., and Gondet, B. (2005) Sulfates in the north polar region of Mars detected by OMEGA/Mars Express. *Science*, 307, 1584–1586.
- Leitner, C., Neubauer, F., Marschallinger, R., Genser, J., and Bernroider, M. (2013) Origin of deformed halite hopper crystals, pseudomorphic anhydrite cubes and polyhalite in Alpine evaporites (Austria, Germany). *International Journal of Earth Sciences*, 102, 813–829.
- Logan, L.M., Hunt G.R., and Salisbury J.W. (1975) The use of mid-infrared spectroscopy in remote sensing of space targets. In C. Karr, Ed., *Infrared and Raman Spectroscopy of Lunar and Terrestrial Minerals*, 117–142. Academic Press, New York.
- Ludwig, C.F. (1804) *Handbuch der Mineralogie nach A.G. Werner* p. Siegfried Lebrecht Crusius, Leipzig.
- Mangold, N., Roach, L., Milliken, R., Le Mouélic, S., Ansan, V., Bibring, J.P., Masson, P., Mustard, J.F., Murchie, S., and Neukum, G. (2010) A Late Amazonian alteration layer related to local volcanism on Mars. *Icarus*, 207, 265–276.
- Massé, M., Bourgeois, O., Le Mouélic, S., Verpoorter, C., Spiga, A., and Le Deit, L. (2012) Wide distribution and glacial origin of polar gypsum on Mars. *Earth and Planetary Science Letters*, 317–318, 44–55.
- McMillan, P.F., and Hofmeister A.M. (1988) Infrared and Raman spectroscopy. In F.C. Hawthorne, Ed., *Spectroscopic Methods in Mineralogy and Geology. Reviews in Mineralogy and Geochemistry*, 18, 99–159.
- Meijer, J.A.M. (1984) Inhibition of calcium sulfate depositions by a fluidized bed. *Desalination*, 52, 25–42.
- Miller, F.A., and Wilkins, C.H. (1952) Infrared spectra and characteristic frequencies of inorganic ions. *Analytical Chemistry*, 24, 1253–1294.
- Miller, F.A., Carlson, G.L., Bentley, F.F., and Jones, W.H. (1960) Infrared spectra of inorganic ions in the cesium bromide region (700–300 cm^{-1}). *Spectrochimica Acta*, 16, 135–235.
- Moenke, H. (1962) *Mineralspektren I: Die Ultrarotabsorption der häufigsten und wirtschaftlich wichtigsten Halogenid-, Oxyd-, Hydroxyd-, Carbonat-, Nitrat-, Borat-, Sulfat-, Chromat-, Wolframat-, Molybdat-, Phosphat-, Arsenat-, Vanadat- und Silikatminerale im Spektralbereich 400–4000 cm^{-1}* . Akademie-Verlag, Berlin.
- Murchie, S.L., Seelos, F.P., Hash, C.D., Humm, D.C., Malaret, E., McGovern, J.A., Choo, T.H., Seelos, K.D., Buczkowski, D.L., Morgan, M.F., and others. (2009) The Compact Reconnaissance Imaging Spectrometer for Mars investigation and data set from the Mars Reconnaissance Orbiter's primary science phase. *Journal of Geophysical Research*, 114, <http://dx.doi.org/10.1029/2009JE003344>.
- Murray, R.C. (1964) Origin and diagenesis of gypsum and anhydrite. *Journal of Sedimentary Petrology*, 34, 512–523.
- Mustard, J.F., and Hays, J.E. (1997) Effects of hyperfine particles on reflectance spectra from 0.3 to 25 μm . *Icarus*, 125, 145–163.
- Ostroff, A.G. (1964) Conversion of gypsum to anhydrite in aqueous salt solutions. *Geochimica et Cosmochimica Acta*, 28, 1363–1372.
- Posnjak, E. (1940) Deposition of calcium sulfate from sea water. *American Journal of Science*, 238, 559–568.
- Prasad, P.S.R., Pradhan, A., and Gowd, T.N. (2001) In situ micro-Raman investigation of dehydration mechanism in natural gypsum. *Current Science*, 80, 1203–1207.
- Prasad, P.S.R., Chaitanya, V.K., Prasad, K.S., and Rao, D.N. (2005) Direct formation of the γ - CaSO_4 phase in dehydration process of gypsum: In situ FTIR study. *American Mineralogist*, 90, 672–678.
- Prothero, D.R., and Schwab F. (2004) *Sedimentary Geology. An Introduction to Sedimentary Rocks and Stratigraphy*. Freeman, New York.
- Ridge, M.J., and Beretka J. (1969) Calcium sulphate hemihydrate and its hydration. *Reviews Pure Applied Chemistry*, 19, 17–44.
- Robertson, E.C., Robie, R.A., and Books, K.G. (1958) Physical properties of salt, anhydrite, and gypsum. Trace Elements Memorandum Report 1048, 38 p. U.S. Geological Survey, Denver.
- Ross, S.D. (1974) Sulphates and other oxy-anions of Group VI. In V.C. Farmer, Ed., *The Infrared Spectra of Minerals*, p. 423–444. The Mineralogical Society, London.
- Ruff, S.W., Christensen, P.R., Barbera, P.W., and Anderson, D.L. (1997) Quantitative thermal emission spectroscopy of minerals: A technique for measurement and calibration. *Journal of Geophysical Research*, 102, 14899–14913.
- Salisbury, J.W. (1993) Mid-infrared spectroscopy: Laboratory data. In C.M. Pieters and P.A.J. Englert, Eds., *Remote Geochemical Analysis: Elemental and Mineralogical Composition*, p. 79–98. Cambridge University Press, U.K.
- Salisbury, J.W., and Wald, A. (1992) The role of volume scattering in reducing spectral contrast of reststrahlen bands in spectra of powdered minerals. *Icarus*, 96, 121–128.
- Salisbury, J.W., Walter, L.S., Vergo, N., and D'Aria, D.M. (1991) *Infrared (2.1–25 μm) Spectra of Minerals*. 267 p. Johns Hopkins University Press, Baltimore.
- Sievert, T., Wolter, A., and Singh, N.B. (2005) Hydration of anhydrite of gypsum ($\text{CaSO}_4\cdot\text{II}$) in a ball mill. *Cement and Concrete Research*, 35, 623–630.
- Singh, M., and Garg, M. (1995) Activation of gypsum anhydrite-slag mixtures. *Cement and Concrete Research*, 25, 332–338.
- Singh, N.B., and Middendorf, B. (2007) Calcium sulphate hemihydrate hydration leading to gypsum crystallization. *Progress in Crystal Growth and Characterization of Materials*, 53, 57–77.
- Squyres, S.W. (2012) Initial Opportunity rover results at Endeavour Crater, Mars. Lunar Planet Science Conference, The Woodlands, Texas, Abstract 1892.
- Squyres, S.W., Arvidson, R.E., Blaney, D.L., Clark, B.C., Crumpler, L., Farrand, W.H., Gorevan, S., Herkenhoff, K.E., Hurowitz, J., Kusak, A., and others. (2006) Rocks of the Columbia Hills. *Journal of Geophysical Research: Planets*, 111, E02S11, <http://dx.doi.org/10.1029/2005JE002562>.
- Sutter, B., Dalton, J.B., Ewing, S.A., Amundson, R., and McKay, C.P. (2007) Terrestrial analogs for interpretation of infrared spectra from the Martian surface and subsurface: Sulfate, nitrate, carbonate, and phyllosilicate-bearing Atacama Desert soils. *Journal of Geophysical Research*, 112, G04S10, <http://dx.doi.org/10.1029/2006JG000313>.
- Szumila, I., Bishop J.L., Fenton L.K., and Brown A.J. (2013) Composition and morphology of gypsum dunes in Olympia Undae on Mars. Lunar Planet Science Conference, The Woodlands, Texas, Abstract 2123.
- Szynkiewicz, A., Ewing, R.C., Moore, C.H., Glamoclija, M., Bustos, D., and Pratt, L.M. (2010) Origin of terrestrial gypsum dunes—Implications for Martian gypsum-rich dunes of Olympia Undae. *Geomorphology*, 121, 69–83.
- Weitz, C.M., Bishop, J.L., and Grant, J.A. (2013) Gypsum, opal, and fluvial channels within a trough of Noctis Labyrinthus, Mars: Implications for aqueous activity during the Late Hesperian to Early Amazonian. *Planetary and Space Science*, 87, 130–145.
- Weitz, C.M., Noe Dobra E.Z., and Wray J.J. (2014) Mixtures of clays and sulfates within deposits in western Melas Chasma. *Icarus*, in press, <http://dx.doi.org/10.1016/j.icarus.2014.04.009>.
- Wenrich, M.L., and Christensen, P.R. (1996) Optical constants of minerals derived from emission spectroscopy: Application to quartz. *Journal of Geophysical Research*, 101, 15921–15931.
- Witzke, A., Arnold, G., and Stöfler, D. (2007) Spectral detectability of Ca- and Mg-sulfates in Martian bright soils in the 4–5 μm wavelength range. *Planetary and Space Science*, 55, 429–440.
- Worke, T., and Parker, A. (1992) Occurrence of bassanite in Lower Lias rocks of the Lyme Regis area, England. *Mineralogical Magazine*, 56, 258–259.
- Wray, J.J., Squyres, S.W., Roach, L.H., Bishop, J.L., Mustard, J.F., and Noe Dobra, E.Z. (2010) Identification of the Ca-sulfate bassanite in Mawrth Vallis, Mars. *Icarus*, 209, 416–421.
- Wray, J.J., Milliken, R.E., Dundas, C.M., Swayze, G.A., Andrews-Hanna, J.C., Baldrige, A.M., Chojnacki, M., Bishop, J.L., Ehlmann, B.L., Murchie, S.L., and others. (2011) Columbus crater and other possible groundwater-fed paleolakes of Terra Sirenum, Mars. *Journal of Geophysical Research*, 116, E01001, <http://dx.doi.org/10.1029/2010JE003694>.
- Yen, A.S., Morris, R.V., Clark, B.C., Gellert, R., Knudson, A.T., Squyres, S., Mittlefehldt, D.W., Ming, D.W., Arvidson, R., McCoy, T., Schmidt, M., Hurowitz, J., Li, R., and Johnson, J.R. (2008) Hydrothermal processes at Gusev Crater: An evaluation of Paso Robles class soils. *Journal of Geophysical Research*, 113, E06S10, <http://dx.doi.org/10.1029/2007JE002978>.
- Zambonini, F. (1910) *Mineralogia Vesuviana. Memorie della Accademia delle scienze, Reale Accademia delle Scienze fisiche e matematiche di Napoli*, 14, 327–328.
- Zhang, Q., Kasai, E., and Saito, F. (1996) Mechanochemical changes in gypsum when dry ground with hydrated minerals. *Powder Technology*, 87, 67–71.